Pergamon

Journal of Structural Geology, Vol. 16, No. 5, pp. 725 to 732, 1994

0191-8141/94 $07.00+0.00

Mechanics of extensional wedges and geometry of normal faults

YI KUN ZHANG

Department of Geology, Research Institute of Petroleum Exploration and Development, P.O. Box 910, Beijing 100083, P.R. China

(*Received* 30 *November* 1992; *accepted in revised form* 15 *June* 1993)

Abstract—Based on the assumption that rocks are fractured simultaneously where the principle stresses reach the critical values of the modified Griffith criterion presented in this paper, a possible formation mechanism for upper crustal extensional wedges is discussed. Regarding the stress in the crust as the superposition of a lithostatic state, in which gravity and fluid pressure are included, and a complementary stress, which possibly implies the superposed tectonic stress, an elastic slab model of the upper crust above the brittle–ductile transition is considered. It is proposed that the strain discontinuity between the failed and unfailed regions in the slab may lead to large-scale curved normal faults, which cannot be explained by traditional fault theory. Three types of extensional wedges are produced, as the magnitude of superposed tensile stress decreases, remains unchanged and increases with depth. Slab length, tensile strength, friction cofficient and fluid pressure, significantly affect the geometry of extensional wedges and their boundary faults.

INTRODUCTION

THE traditional Andersonian fault theory, which is based on the shear failure criterion and directions of principle stresses, cannot explain normal faults revealed by seismic sections in sedimentary basins related to crustal extension, or field work on the Basin and Range tectonics. Two features are found characterizing these normal faults, which are inconsistent with this theory. First, the faults are usually curved in shape and at a low-angle (Wernicke 1981, Wernicke and Burchfiel 1983). Second, the faults are accompanied by very complex internal deformation within either hangingwall or footwall (White *et al.* 1986, Wernicke & Axen 1988). Recent work on these normal faults explains them in terms of an extensional wedge (Xiao *et al.* 1991). However, the cause of these normal faults is still controversial, because a mechanical insight into their development has not been provided.

In the geological definition of a fault, it is claimed that there must be relative displacement between two blocks. The complete description of a fault should include the pre-failure and the post-failure stress–strain relationship of rocks in conjunction with a failure criterion. Such a description would, of course, be mechanically complicated because these parameters are time-dependent and space-dependent. It is therefore reasonable to look for a theoretical approach that can at least model some features of rock deformation with fair precision, although the physical interpretation may be less precise. For this purpose, two assumptions are made. (a) Tensile stresses are applied to a homogeneous elastic material; failure happens simultaneously in the material where the principle stresses reach the critical value of a failure criterion. (b) As soon as the failure takes place, the elastic energy in the material is released, and the inelastic strain along numerous failure planes is assumed to dominate the mechanical behaviour of the fractured material.

Because of rigidity of upper crustal rocks, a large amount of crustal deformation, especially the lateral strain, cannot be elastic strain occurring before failure. Large deformation only occurs during the post-failure stage and within the failure region of the upper crust. Consequently, there must be strain discontinuity at the boundary between the failure region, in which rocks are fractured, and the rigid region, in which rocks remain rigid and deform elastically but only by a small amount. The discontinuity could be identified in geological sections as a fault. In this view, a fault is the boundary of the failure region, whose geometry is mechanically determined.

Geological faults are usually thought to be restricted to the upper crust above the depth of the brittle–ductile transition. Below that depth, the lower crust is assumed to be always ductile. The mechanical model that will be discussed here is assumed to be valid above that depth. With these specifications, the paper sets out, first, to calculate elastic stresses in the upper crust before failure. Then, a failure criterion is applied to determine the failure region and finally the fault geometry.

MECHANICAL MODEL

Lithostatic state

Hafner (1951) expressed the stresses in the crust to be the superposition of stress caused by gravity and a complementary stress, known as the principle of superposition of stresses. The stress caused by gravity is calculated by assuming that lateral extension is prevented. The relation,

$$\sigma_x = \sigma_y = \nu\sigma_z/(1-\nu)$$

is derived, where ν is Poisson's ratio, σ_x and σ_y are the two horizontal stresses, and σ_z is the vertical stress

caused by gravity. The horizontal stresses are only a third of the vertical stress as the Poisson's ratio of rocks is usually taken to be 0.25. This is the case in which the effect of fluid pressure is not considered.

When fluid pressure is in effect, the general form of stress–strain relationship should be as follows (see Jaeger & Cook 1979),

$$\begin{cases} E\varepsilon_x = \sigma_x - \nu(\sigma_y + \sigma_z) - p(E/3H) \\ E\varepsilon_y = \sigma_y - \nu(\sigma_x + \sigma_z) - p(E/3H), \\ E\varepsilon_z = \sigma_z - \nu(\sigma_x + \sigma_y) - p(E/3H) \end{cases} \quad (1)$$

where H is a constant and p is fluid pressure. If fluid pressure is assumed to vary with depth, and is invariable in the horizontal directions, similarly letting $\varepsilon_x = \varepsilon_y = 0$ as the lateral strain is prevented, we obtain,

$$\sigma_x = \sigma_y = \nu\sigma_z/(1 - \nu) + pE/(3(1 - \nu)H). \quad (2)$$

Here the equilibrium and compatible equations are automatically satisfied by setting shear stresses to be zero. Equation (2) is also a valid solution in the two-dimensional case of plain strain.

According to the assumption made by Biot (1941), $E/H = 3(1-2\nu)$. Let $\nu = 0.25$, we finally obtain,

$$\begin{cases} \sigma_x = \sigma_y = (1 + 2\alpha)\sigma_z/3 \\ \sigma_z = \rho\mathbf{g}z \\ \alpha = p/\sigma_z, \end{cases} \quad (3)$$

where α represents the coefficient of fluid pressure. It is obvious that the standard state, $\sigma_x = \sigma_y = \sigma_z$, originally introduced by Anderson (1942), is possible only when $\alpha = 1$. For a normal gradient of fluid pressure, $\alpha = 0.4$, the horizontal stresses are 60% of the vertical stress. If $\alpha = 0$, it is the case where the effect of fluid pressure is not considered.

On the other hand, because the compatible equations and equilibrium equations are the linear differential equations of stress components and fluid pressure, the superposition law is always valid. Therefore, if a lithostatic state is defined, in which gravity and fluid pressure are assumed to be the source of stresses and lateral strain is prevented, then, the stresses in the crust can be described as the superposition of the stresses of lithostatic state and the complementary stresses. The lithostatic stresses have been found to be equation (3). It remains to determine complementary stresses.

Pre-failure elastic stress

Hafner (1951) obtained the polynomial solution of elastic stresses in a block under compression and shearing by using the Airy stress function. In this study, we consider a similar slab model with horizontal length L and vertical thickness D, but under tension and shearing. We confine the discussions to two dimensions and set the co-ordinate axes, x and z, illustrated in Fig. 1(a). The slab is assumed to be in lithostatic equilibrium when no additional stress is superimposed on it. The slab

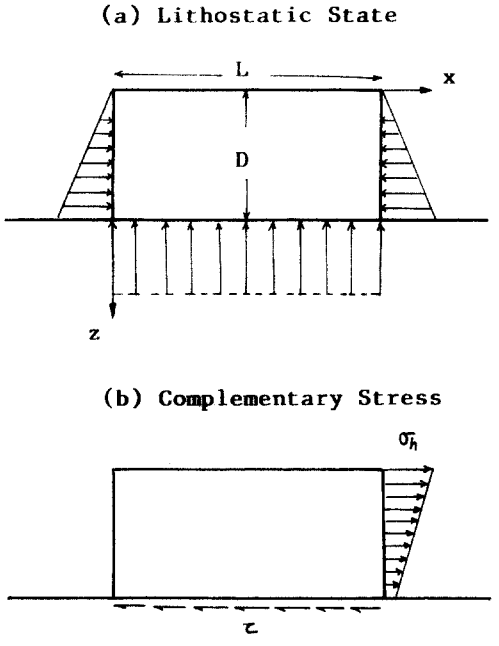

Fig. 1. A slab model of the upper crust under tensile stress. The stress in the slab can be regarded as the superposition of (a) lithostatic state in which only gravity and fluid pressure are considered and (b) the complementary stress. See text.

is pulled along its right-hand edge by a horizontal tensile stress σ_h (see Fig. 1b). Letting σ_h change linearly with the depth,

$$\sigma_h = \sigma_0 + kz, \quad (4)$$

where σ_0 and k are constants.

The boundary conditions of the slab are as follows: on the left side of the slab, both σ_x and σ_z are unaffected by the tensile stress σ_h and equal to the lithostatic pressure, $(1 + 2\alpha)\rho\mathbf{g}z/3$ and $\rho\mathbf{g}z$, respectively; on the right side of the slab σ_x is assumed to be the sum of lithostatic pressure and the superimposed tensile stress σ_h, while σ_z is still equal to the lithostatic pressure, $\rho\mathbf{g}z$. At the surface, the stress σ_z is always equal to zero, and the shear stress τ_{xz} is also always equal to zero. At the bottom, the slab suffers a constant shear stress $\tau_{xz} = \tau$, which is necessary to slab equilibrium, and the vertical for stress $\sigma_z = \rho\mathbf{g}D$ along this boundary.

The complementary stresses for this two-dimensional problem can be found analytically. The Airy stress function U is,

$$U = kxz^3/(6L) + \sigma_0 xz^2/(2L). \quad (5)$$

On the basis of the principle of superposition, we have the stresses in the slab,

$$\sigma_x = kxz/L + \sigma_0 x/L + (1 + 2\alpha)\rho\mathbf{g}z/3 \quad (6)$$

$$\sigma_z = \rho\mathbf{g}z \quad (7)$$

$$\tau_{xz} = -kz^2/(2L) - \sigma_0 z/L, \quad (8)$$

where ρ is the density of crust, $\mathbf{g}$ is the gravity acceleration. By equations (6), (7) and (8), it is indicated that the slab thickness D has no effect on elastic stresses. The shear stress is independent of the horizontal co-ordinate.

Failure criterion

A modified Griffith criterion is adopted here. As is generally accepted, the Griffith cracks in materials will be closed when the normal stress on the cracks reaches a critical value and the fracture will take place in the form of frictional slip along the closed crack surfaces, which could be described by the Coulomb criterion. Three physical parameters, tensile strength T_0, friction coefficient μ, and the critical stress σ_c control this process. In this study, the critical stress σ_c is solved geometrically from the tensile strength T_0 and friction coefficient μ by keeping the Mohr envelope of the Coulomb criterion with the friction coefficient μ in tangent with the envelope of the Griffith criterion with the tensile strength T_0 (Fig. 2). In this way, the critical stress σ_c and the inherent shear strength S_0 can be expressed in T_0 and μ by solving the equations of the Griffith criterion, $\tau^2 = 4T_0(\sigma + T_0)$, and the Coulomb criterion, $\tau = S_0 + \mu\sigma$. We have,

$$\sigma_c = (1/\mu^2 - 1)T_0 \tag{9}$$

$$S_0 = (1/\mu + \mu)T_0. \tag{10}$$

It is of note that if the inherent shear strength S_0 in equation (10) is equal to that implied by the modified Griffith theory of McClintock & Walsh (1962), $2T_0(1 + \sigma_c/T_0)^{1/2} - \mu\sigma_c$, the geometrically determined normal stress at the tangent point in Fig. 2 is just the critical stress defined by McClintock & Walsh (1962). Therefore, the present modified Griffith failure criterion is not merely geometrical, but may have some mechanical basis. The benefit of the present criterion is that the continuity of the Mohr envelope is preserved. By taking account of the effect of fluid pressure, the failure criterion can be written in the form of effective normal stress and shear stress,

$$\tau^2 = 4T_0(\bar{\sigma} + T_0) \qquad \bar{\sigma} \le (1/\mu^2 - 1)T_0 \tag{11}$$

$$\tau = (1/\mu + \mu)T_0 + \mu\bar{\sigma} \qquad \bar{\sigma} > (1/\mu^2 - 1)T_0. \tag{12}$$

Four physical parameters T_0, μ, α and ρ in equations (6)–(12) must be given appropriate values. Estimates of tensile strength T_0 from laboratory experiments for crystalline rocks (Brace 1964, Jaeger & Cook 1979) lie predominantly in the range 10–40 MPa. A mean value $T_0 = 20$ MPa is chosen. The coefficient of friction μ from laboratory experiments (Byerlee 1978, Jaeger & Cook 1979) lie predominantly in the range of 0.5–1.0. Also a mean value $\mu = 0.75$ is chosen. The density of crust is chosen to be 2550 kg m^{-3}, which gives the usually adopted geopressure gradient, 25 MPa km^{-1}. A normal fluid pressure gradient, 10 MPa km^{-1}, is used in this study, which gives the coefficient, $\alpha = 0.4$.

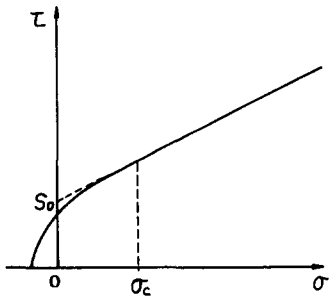

Fig. 2. The Mohr envelope of the modified Griffith criterion. See text.

EXTENSIONAL WEDGES

An elastic slab model has been introduced to describe the pre-failure mechanical behaviour of rocks composing the upper crust. The rocks are fractured when the shear stress reaches the critical value of (11) or (12). On the basis of the simultaneous failure hypothesis made at the beginning of the paper, the failure region in the slab would be determined in the combination of equations (6)–(12). The following three cases of horizontal tensile stress σ_h are considered:

(a) the magnitude of σ_h linearly decreases with depth;
(b) the magnitude of σ_h is invariable with the depth;
(c) the magnitude of σ_h linearly increases with depth.

In case (a), σ_h should vanish at the depth of brittle–ductile transition (25 km assumed in the following calculations), by taking account of the fact that the ductile lower crust is incapable of bearing significant elastic stress. In case (c), σ_h is assumed to be equal to zero at the surface.

When σ_h is given, the elastic stresses in the slab are calculated from equations (6)–(8) on grids, 0.2×0.2 km. The stresses are transformed into principal stresses. Then, the failure criterion, equations (11) and (12), is used to determine whether a grid area is fractured. If a grid is fractured, the two conjugate orientations of failure are calculated in combination with the directions of principal stresses.

Figure 3 displays the results for the above three cases for an upper crustal slab, 25 km in the thickness and 50 km in the length. The applied tensile stresses are, respectively,

(a) $\sigma_h = -250 + 10z$ (MPa, km)
(b) $\sigma_h = -65$ (MPa)
(c) $\sigma_h = -15z$ (MPa, km).

The areas marked with failure orientations are the failed regions. Three types of extensional wedges with different styles of the boundary faults which separate the failed and unfailed regions are shown.

In the case of the magnitude of σ_h decreasing with depth, a wedge on a typical listric fault is exhibited (Fig. 3a). The boundary fault intersects the surface at the dip about 45° and flattens to the dip about 10° below the depth of 15 km. In the case of the magnitude of σ_h invariable with depth (Fig. 3b), the wedge is shown on a low-angle fault at the dip of 15° above the depth of 5 km, and on a steeper fault at the dip about 50° below 10 km. The boundary fault is convex upward. In the case of the magnitude of σ_h increasing with depth, the geometry of extensional wedge is completely changed. The boundary fault seems to be in the mirror relationship to that in Fig. 3(a) and footwall is the failed region (Fig. 3c).

The type of fault in Fig. 3(a), known as a detachment

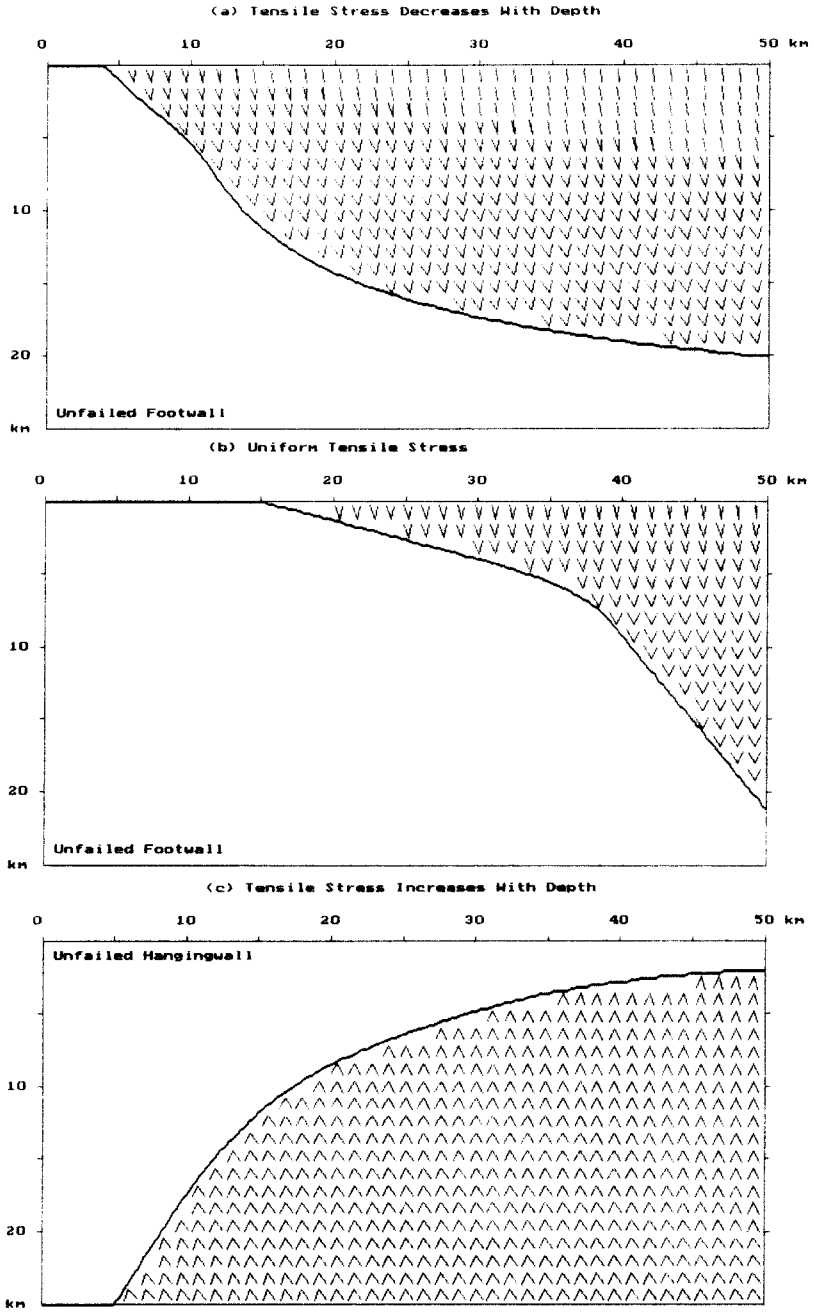

Fig. 3. Geometry of extensional wedges and their boundary faults calculated with different rules for tensile stress σ_h and $T_0 = 20$ MPa, $\mu = 0.75$, $\alpha = 0.4$. For full details and discussion, see text.

fault, was reported as prevailing in extensional basins (e.g. Le Pichon & Barbier 1987, Etheridge *et al.* 1989, William 1991, Xiao & Suppe 1992). The present mechanical model provides a physical insight into detachment faulting. Another feature revealed by the present model is that the vertical distribution of horizontal tensile stress σ_h controls whether the hangingwall or the footwall of boundary fault deforms inelastically depending on whether the extensional wedge is above or below the boundary fault. In the cases of Figs. 3(a) & (b), the hangingwall is the extensional wedge and will be capable of inelastic response to the slab deformation, while in the case of Fig. 3(c), the footwall is the extensional wedge.

Based on geometrical considerations of hangingwall deformation, White *et al.* (1986) proposed inclined simple shear in the hangingwall to challenge the vertical simple shear assumption under gravity collapse (e.g. Gibbs 1983) and gave a kinematic method to construct bed from fault, or fault from bed. Footwall inelastic response to lateral extension was first proposed by Wernicke & Axen (1988) as another challenge to the traditional assumption of hangingwall collapse. As the inelastic strain of an extensional wedge is concerned with the post-failure stage, the internal deformation is generally very complex (e.g. Waltham 1989, McClay 1990). There may not be a single shear angle. If further deformation of extensional wedge in the post-failure stage takes place along numerous failure planes, as assumed at the beginning of the paper, there are two

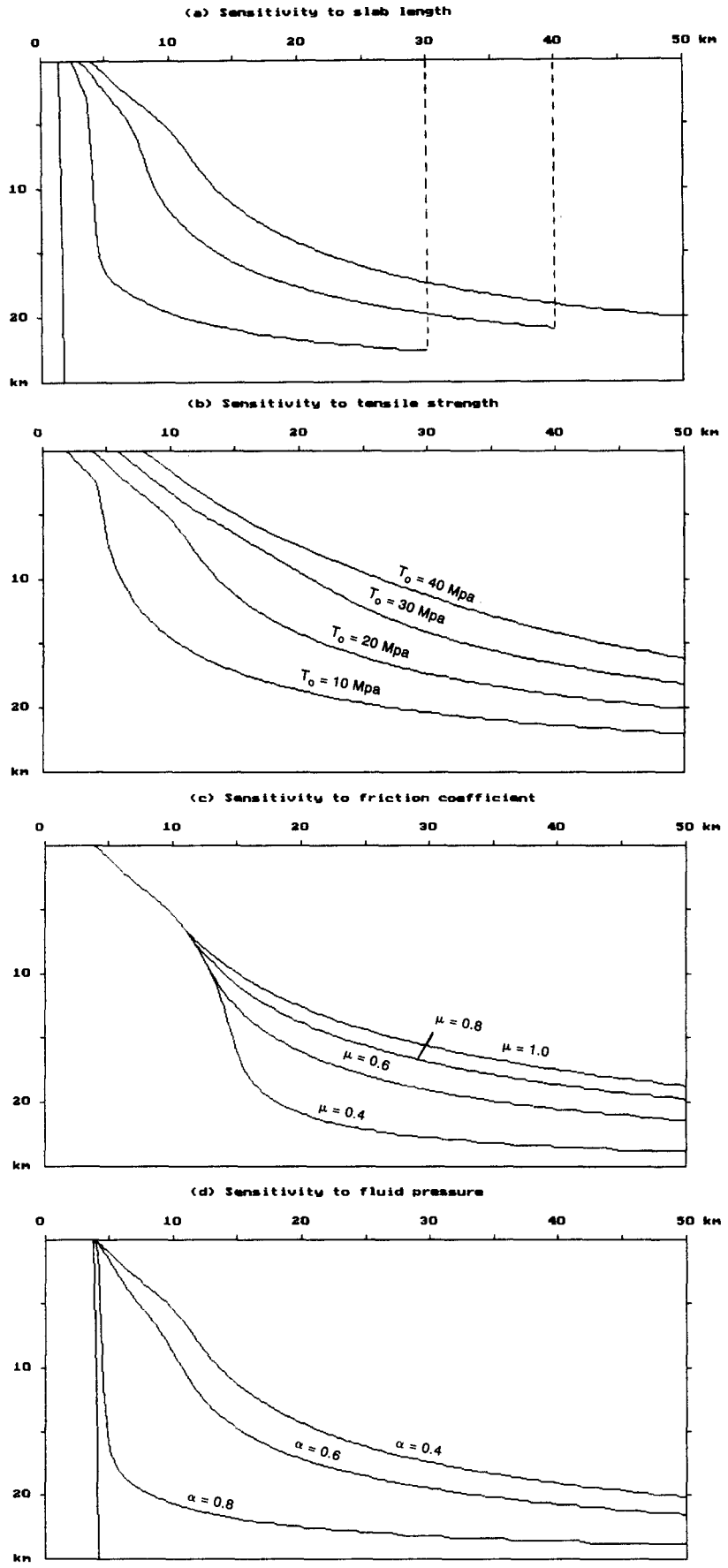

Fig. 4. Sensitivity of fault geometry to parameters. $\sigma_h = -250+10z$ (MPa, km), $T_0 = 20$ MPa, $\mu = 0.75$, $\alpha = 0.4$. (a) Only slab length is changed. (b) Only tensile strength is changed. (c) Only friction coefficient is changed. (d) Only fluid pressure is changed.

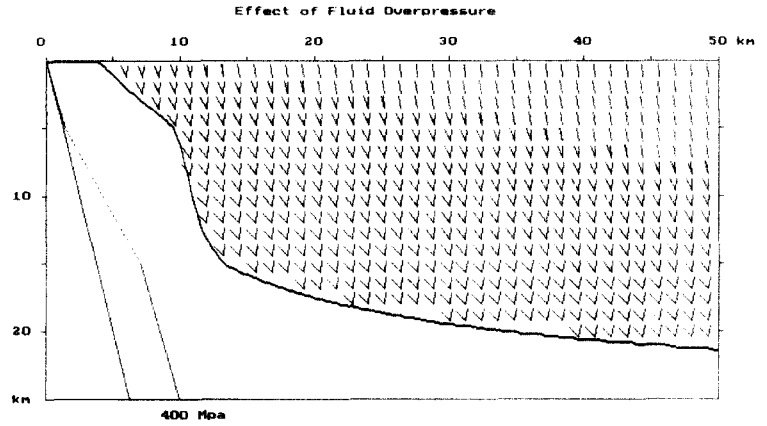

Fig. 5. The effect of fluid overpressure on fault geometry. $\sigma_h = -250 + 10z$ (MPa, km), $T_0 = 20$ MPa, $\mu = 0.75$. At a depth of 5–15 km, the fluid overpressure significantly changes the shape of boundary fault compared to Fig. 3(a).

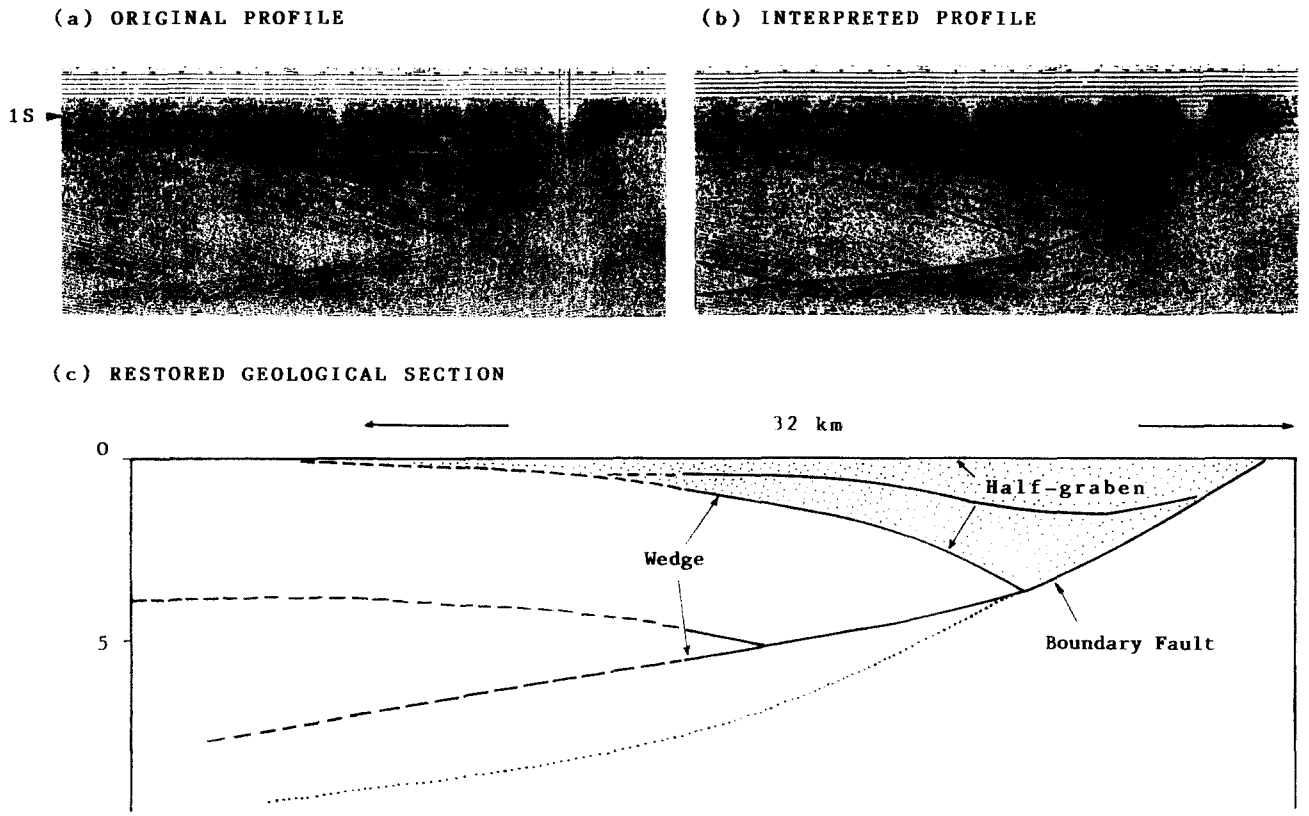

Fig. 6. A large-scale low-angle normal fault in the Bohai Gulf of North China (seismic profile: YX 519.9) (a) Original seismic profile. (b) Interpreted seismic profile. (c) Restored geological section at the end of extension. The dashed lines are speculated. The predicted shape of the fault is marked by the dotted line. See text.

main conjugate failure trajectories shown in Fig. 3. In the case of Fig. 3(a), one failure trajectory at a dip of about 45° exhibits a fair continuity which may develop and become the second faults in the hangingwall.

DISCUSSION

The geometry of boundary faults of extensional wedges determines the basin structure, so is commercially worthy of study. In Fig. 3, the vertical distribution of σ_h is shown to control the geometrical style of extensional wedges. But what about the effects of other parameters on the fault geometry? In Fig. 4, under the same tensile stress σ_h as that in Fig. 3(a), the sensitivity of fault geometry to other parameters is illustrated.

Figure 4(a) illustrates the fault geometry with slab length L = 50, 40, 30 and 20 km. The fault becomes steeper as the slab becomes shorter. When slab length decreases to 20 km, nearly the whole slab will be fractured under this tensile stress. The tensile stress to produce a wedge certainly decreases with decrease in the length. Figure 4(b) exhibits the fault geometry with tensile strength T_0 = 10, 20, 30 and 40 MPa. The fault seems to be more sensitive to tensile strength when tensile strength is less than 20 MPa. As tensile strength

increases, the slab becomes strong and the wedge becomes shallow. The effect of friction on fault geometry is shown in Fig. 4(c), using friction coefficient $\mu = 0.4, 0.6, 0.8$ and 1.0. It is clear that the friction coefficient only changes the geometry of the fault at depth. In Fig. 4(d), fluid pressure is shown to drastically change the geometry of the fault, especially when $\alpha > 0.6$. The tensile stress to drive a wedge will significantly decrease when a high fluid pressure is presented. The effect of fluid overpressure on fault geometry is shown in Fig. 5. The fault becomes steep where the fluid overpressure exists.

In the Bohai Gulf of North China, there are more than 50 half-grabens discovered by petroleum exploration. Each half-graben called a depression is limited by a boundary fault (e.g. Li 1982). The mechanical model that has been discussed is applied to a typical seismic section demonstrating a large-scale low-angle normal fault developed in Yangxing Depression of the Gulf (Fig. 6a). The reflection on the fault is strong and clear. Four beds marked with the solid lines are interpreted (Fig. 6b). The fault intersects the surface at the dip about 35°. By backstripping the post-extension sediments on the top, the restored geological section at the end of extension is obtained (Fig. 6c). The dashed line part of the section is inferred according to the structural trends of the beds and the fault. The amount of horizontal extension is measured to be about 8 km. The width of the half-graben is estimated from the section to be about 40 km. Assuming $L = 32$ km, $T_0 = 20$ MPa, $\mu = 0.75$, $\alpha = 0.4$ and $\sigma_h = -125 + 8z$ (MPa, km), the best-fit fault geometry is the dotted curve in Fig. 6(c). There is a significant discrepancy between the predicted fault and interpreted fault, which cannot be avoided within the range of possible model parameters. The discrepancy probably resulted from the uplift of extensional wedge under isostasy during the post-failure stage.

Several limitations in the present model needed to be stated so that the modelling results are not over interpreted. First, the predicted boundary faults of extensional wedges only represent the initial geometry of the faults. It will certainly be reshaped during the post-failure deformation. Second, the simultaneous failure hypothesis reduces the problem to a theoretical one. Dropping the hypothesis for a more realistic approach requires the effects of stress propagation and concentration to be considered, which is not easy to formulate. Third, the model depends on four unknown parameters: T_0, μ, α and σ_h, and the only thing that can be compared to real data is the shape of fault plane so the conclusions are highly model dependent and poorly constrained.

The tensile stress σ_h considered in the paper is the complementary stress in reference to the lithostatic state, which possibly implies the tectonic stress superposed on the right-hand end of the slab. The required magnitudes of σ_h to drive the extensional wedges in Fig. 3 are, on average, 125, 65 and 150 MPa. These numbers are greater than the usually estimated magnitudes of lithospheric tectonic stresses (e.g. 50 MPa is the upper limit of ridge push, Kusznir & Park 1984). It must be noted that the tensile stress considered in the paper should be regarded as the extreme stress of the upper crustal slab before the failure happens. It dies out as soon as the failure takes place. Geophysically, there are several possibilities to produce such a great tensile stress. The bending of an elastic upper crustal slab could provide enough tensile stresses to cause the fracture considered in the present model. The bending moment may be the result of an isostatic response to a load (e.g. Walcott 1970). When the slab moves on the non-spherical Earth surface as assumed in plate tectonics, the membrane stress estimated by Turcotte & Oxburgh (1973) exceeds the maximum stress magnitude calculated in this paper. In a rift basin, the thermal stress originating from heat transfer in the lithosphere also provides enough tensile stress (Reiter & Minier 1985).

Acknowledgements—I thank an anonymous reviewer and H. Xiao for constructive and extensive comments on the manuscript, which helped me to compose the revised version. I also thank my colleague, Ms H. Tang, for drawing the figures.

REFERENCES

Anderson, E. M. 1942. *The Dynamics of Faulting*. Oliver and Boyd, London.

Biot, M. A. 1941. General theory of three-dimensional consolidation. *J. appl. Phys.* **12**, 155–164.

Brace, W. F. 1964. Brittle fracture of rocks. In: *State of Stress in the Earth's Crust* (edited by Judd, W. R.). Elsevier, New York.

Byerlee, J. D. 1978. Friction of rocks. *Pure & Appl. Geophys.* **116**, 615–626.

Etheridge, M. A., Symonds, P. A. & Lister, G. S. 1989. Application of detachment model to reconstruction of conjugate passive margins. In: *Extensional Tectonics and Stratigraphy of the North Atlantic Margins* (edited by Tankard, A. J. & Balkwill, H. R.). *Mem. Am. Ass. Petrol. Geol.* **46**, 23–40.

Gibbs, A. D. 1983. Balanced cross-section construction from seismic sections in areas of extensional tectonics. *J. Struct. Geol.* **5**, 153–160.

Hafner, W. 1951. Stress distributions and faulting. *Bull. geol. Soc. Am.* **62**, 373–398.

Jaeger, J. C. & Cook, N. G. W. 1979. *Fundamentals of Rock Mechanics*. Chapman and Hall, London.

Kusznir, N. J. & Park, R. G. 1984. Intraplate lithosphere deformation and the strength of the lithosphere. *Geophys. J. R. astr. Soc.* **79**, 513–538.

Le Pichon, X. & Barbier, F. 1987. passive margin formation by low-angle faulting within the upper crust: The Nothern Bay of Biscay Margin. *Tectonics* **6**, 133–150.

Li, D. S. 1982. Geological structure and hydrocarbon occurrence of the Bohai Gulf oil and gas basin. In: *Petroleum Geology in China* (edited by Mason, J. F.). Penn Well Books, Oklahoma.

McClay, K. R. 1990. Extensional fault systems in sedimentary basins: a review of analogue model studies. *Mar. & Petrol. Geol.* **7**, 206–233.

McClintock, F. A. & Walsh, J. B. 1962. Friction on Griffith cracks under pressure. *Fourth U.S. Nat. Congress. of Appl. Mech. Proc.*, 1015–1021.

Reiter, M. & Minier, J. 1985. Possible influences of thermal stresses on Basin and Range faulting. *J. geophys. Res.* **90**, 10,209–10,222.

Turcotte, D. L. & Oxburgh, E. R. 1973. Mid-plate tectonics. *Nature* **244**, 337–339.

Walcott, R. I. 1970. Flexure of the lithosphere at Hawaii. *Tectonophysics* **9**, 435–446.

Waltham, D. 1989. Finite difference modelling of hangingwall deformation. *J. Struct. Geol.* **11**, 433–437.

Wernicke, B. 1981. Low-angle normal faults in the Basin and Range province: Nappe tectonics in an extending orogen. *Nature* **291**, 645–648.

Wernicke, B. & Axen, G. J. 1988. On the role of isostasy in the evolution of normal fault systems. *Geology* **16**, 848–851.
Wernicke, B. & Burchfiel, B. C. 1983. Modes of extensional tectonics. *J. Struct. Geol.* **4**, 105–115.
White, N. J., Jackson, J. A. & McKenzie, D. P. 1986. The relationship between the geometry of normal faults and that of sedimentary layers in their hangingwalls. *J. Struct. Geol.* **8**, 897–910.
William, F. D. 1991. Geometric models of listric normal faults and rollover folds. *Bull. Am. Ass. Petrol. Geol.* **75**, 1609–1625.
Xiao, H., Dahlen, F. A. & Suppe, J. 1991. Mechanics of extensional wedges. *J. geophys. Res.* **96**, 10,301–10,318.
Xiao, H. & Suppe, J. 1992. Origin of rollover. *Bull. Am. Ass. Petrol. Geol.* **76**, 509–519.